Edge Detail Preservation Technique for Enhancing Speckle Reduction Filtering Performance in Medical Ultrasound Imaging

Yasser M. Kadah[1], Ahmed F. Elnokrashy[2]
Electrical and Computer Engineering Department, King Abdulaziz University, Jeddah, Saudi Arabia[1]
Biomedical Engineering Department, Cairo University, Giza, Egypt[1]
Electrical Engineering Department, Benha University, Benha, Egypt[2]
Computer Science Department-Faculty of Information Technology and Computer Science, Nile University, Giza, Egypt[2]

***Abstract*—Ultrasound imaging is a unique medical imaging modality due to its clinical versatility, manageable biological effects, and low cost. However, a significant limitation of ultrasound imaging is the noisy appearance of its images due to speckle noise, which reduces image quality and hence makes diagnosis more challenging. Consequently, this problem received interest from many research groups and many methods have been proposed for speckle suppression using various filtering techniques. The common problem with such methods is that they tend to distort the edge detail content within the image and blurring is commonly encountered. In this work, we propose a new method that could be combined with previous speckle suppression techniques to preserve edge detail content of the image. The original image is first processed to extract the edge detail content. Rather than presenting the original method to the speckle suppression filtering technique, the edge detail content is subtracted from the original image before it is filtered. Then, such edge detail content is added to the output of filtering to form the final image. The new method is practically verified using 26 imaging experiments as well as ultrasound images from publicly available databases in combination with four widely used speckle reduction filters. The results are evaluated qualitatively and quantitatively using standard image quality metrics.**

Keywords*—*Edge detail preservation; image quality metrics; speckle reduction; ultrasound imaging

I. Introduction

Ultrasound imaging stands out as a widely embraced clinical imaging technique, lauded for its safety, cost-effectiveness, and diverse soft tissue imaging applications encompassing abdominal imaging, echocardiography, and obstetrics and gynecology [1]. The mechanism involves emitting low-intensity acoustic wave pulses into the body, capturing the reflected and scattered echoes from internal structures to construct a cross-sectional anatomical image. With its inherent safety and an impeccable track record in clinical applications, ultrasound imaging stakes its claim as the safest imaging modality to date. Its prevalence in critical applications, such as monitoring fetal growth and assessing biophysical profiles during pregnancy, attests to its reliability. The technology spans a spectrum, ranging from basic handheld units costing a few thousand dollars to sophisticated systems tailored for specialized applications like echocardiography, commanding prices in the hundreds of thousands. This versatility ensures accessibility in rural and low-income communities and integration into large, specialized hospitals, poised to become as indispensable to medical practice as the stethoscope.

Despite the myriad advantages of ultrasound imaging, a glaring issue persists in the quality of its images compared to other modalities. The visual noise and the requisite training to correlate anatomy with ultrasound images stem from speckle, a persistent problem since the inception of ultrasound imaging. Research efforts, both academic and industrial, have focused on mitigating speckle noise in ultrasound images due to its undeniable impact on the technology [2].

Speckle noise emerges inevitably as a direct consequence of the underlying physics in ultrasound imaging. The process involves transmitting an ultrasonic pulse through the body using a 1D or 2D array-formatted ultrasonic transducer. This pulse propagates through tissues, engaging with their various components, resulting in reflected waves from specular reflectors and scattering from point reflectors [1]. The distinguishing factor between specular and point reflectors lies mainly in size; specular reflectors surpass the ultrasound wavelength, while scatterers are notably smaller than this wavelength, typically a fraction of a millimeter within the 2-15 MHz range of ultrasound imaging frequencies. Consequently, tissue interfaces and major blood vessels mimic specular reflectors, while blood capillaries and cells within the extracellular space act as scatterers [3][4]. In tissues like the liver, hepatocytes independently scatter ultrasound waves, with the backscattered part received by the ultrasound transducer. Given the dependence on ultrasound transducer frequency, orientation, and the intricate 3D tissue structure, the received scattered waves from myriad cells interfere, creating a pattern of partial constructive and destructive interference points that manifest as random noise in the image. The crucial disparity between speckle noise and true random noise lies in the former's persistence under unaltered imaging conditions, resisting improvement through averaging or conventional methods [5][6].

Numerous approaches have been proposed to tackle the challenge of speckle reduction, broadly categorized as either acquisition or post-processing methods. Acquisition methods aim to diminish speckle by acquiring multiple versions of the

same slice with varying beamforming parameters, such as steering, focal point, and frequency [7] [8]. Although this approach appears straightforward, its practical implementation demands the reprogramming of acquisition protocols for different applications, incurring substantial costs and posing challenges in applications requiring high frame rates or specific acquisition sequences, such as in 3D and 4D imaging [8]. Alternatively, the second approach, centered on postprocessing, has garnered attention from research groups since the 1980s. The fundamental premise involves commencing with the acquired image and applying diverse filtering strategies to suppress speckle noise. This approach mandates only a digital processing platform and access to the ultrasound imaging system's frame buffer. It can also operate on an external computer with a frame grabber or other means to collect ultrasound images without altering the existing system. Given the advancements in modern computing platforms, including parallel processing and GPUs, this approach emerges as the pragmatic starting point for practical purposes with existing ultrasound imaging systems. Technically, most classical post-processing methods fall into four main categories, with hybrids across them—linear, nonlinear, diffusion-based, and wavelet-based filtering methods [2]. Linear filters encompass techniques like first-order statistics filtering, local statistics filtering with higher moments, and homogeneous mask area filtering [9], [10], [11]. Nonlinear filtering methods include median filtering, linear scaling filter, geometric filtering, and homomorphic filtering [12], [13], [14], [15]. Diffusion-based methods include various variants of anisotropic diffusion filtering [16], [17], [18], [19], [20]. Wavelet-based methods primarily operate using wavelet shrinkage with different wavelet families and levels of composition [21], [22], [23], [24]. Hybrids incorporating elements from these methods have also been introduced [25], [26], [34], [35]. Other approaches include methods that use a human visual system model to reduce the appearance of noise in ultrasound images [36], and methods involving deep learning using convolutional neural networks to build despeckling models from training custom-designed networks [37], [38].

Despite the strides made in speckle reduction methods, challenges persist in bridging the gap between the perceived quality of processed images by researchers and clinicians. The apparent smoothness achieved by these methods may compromise crucial edge details, significant to clinical sonographers. To harness the full potential of existing techniques, there is an imperative to enhance their performance and align them more accurately with the clinical perspective on image quality [27]. Recognizing the substantial contributions of current techniques is vital, but addressing their common shortcomings is crucial to maximizing their efficacy in routine clinical ultrasound applications.

In this work, we propose a new method that could be combined with previous speckle suppression techniques to preserve edge detail content of the image. The original image is first processed to extract the edge detail content. Rather than presenting the original method to the speckle suppression filtering technique, the edge detail content is subtracted from the original image before it is filtered. Then, such edge detail content is added to the output of filtering to form the final image. The new method is experimentally verified using 26 imaging experiments as well as ultrasound images from publicly available databases with four widely used speckle reduction filters. The results are evaluated qualitatively and quantitatively using image quality metrics.

II. METHODOLOGY

Ultrasound image acquisition involves gathering a series of lines (or sticks) extending across the scanned area, arranged either linearly or in a sector pattern, contingent upon the employed imaging probe. The acquired data, referred to as stick data, serves as the foundation for generating a properly formatted output image through image reconstruction techniques, leveraging the provided geometry information. The new method starts from estimating the edge detail content from the original stick data. It works by applying edge detection techniques such as Canny edge detection to the original stick data to generate a map of the locations of salient edge detail features [27]. To better include the complete edge detail features and take into account having a smooth transition to their surroundings in the subsequent steps, the generated edge map is blurred using a simple spatial domain filtering with a Gaussian kernel. The normalized version of the outcome is used as a mask that is multiplied by the original stick data to extract the edge detail content. A version of the original stick data that contains only the edge detail-free parts of the data is computed by subtracting such edge detail content from the original stick data. The detail-free data is used as the input to the speckle reduction filtering method. The restoration of edge detail content to the filtering output is done by adding them. The basic block diagram of the new edge detail preservation method is shown in Fig. 1. In order to visually illustrate the steps of the process, example stick data for all steps of the process are presented in Fig. 2 with comparison to the stick data output from the original speckle filtering alone.

The implementation and testing of the novel edge detail preservation method involved four widely adopted speckle reduction filtering techniques, serving as representative examples from each of the four primary post-processing categories, without sacrificing generality. These techniques were wavelet denoising [21], [23], relaxed median (RMedian) denoising [14], [15], speckle reducing anisotropic diffusion (SRAD) [17], [16], [18], and local statistics based filtering (Lee) [9], [10]. In each of these techniques, the original technique is implemented with the implementation details suggested in the most recent variant. In order to quantitatively assess the image quality improvement, eleven image quality metrics are compared between the original filtering technique alone and its combination with the new edge detail preservation method. The image quality metrics used are geometric absolute error (GAE) [2], mean-squared error (MSE) [2], Laplacian mean-squared error (LMSE) [28], normalized absolute error (NAE) [28], Minkowski error metric (for β=1, 3, 4) [29], universal quality index (Q) [30], structural similarity index (SSIN) [29], signal-to-noise ratio (SNR) [31], and peak signal-to-noise ratio (PSNR) [31].

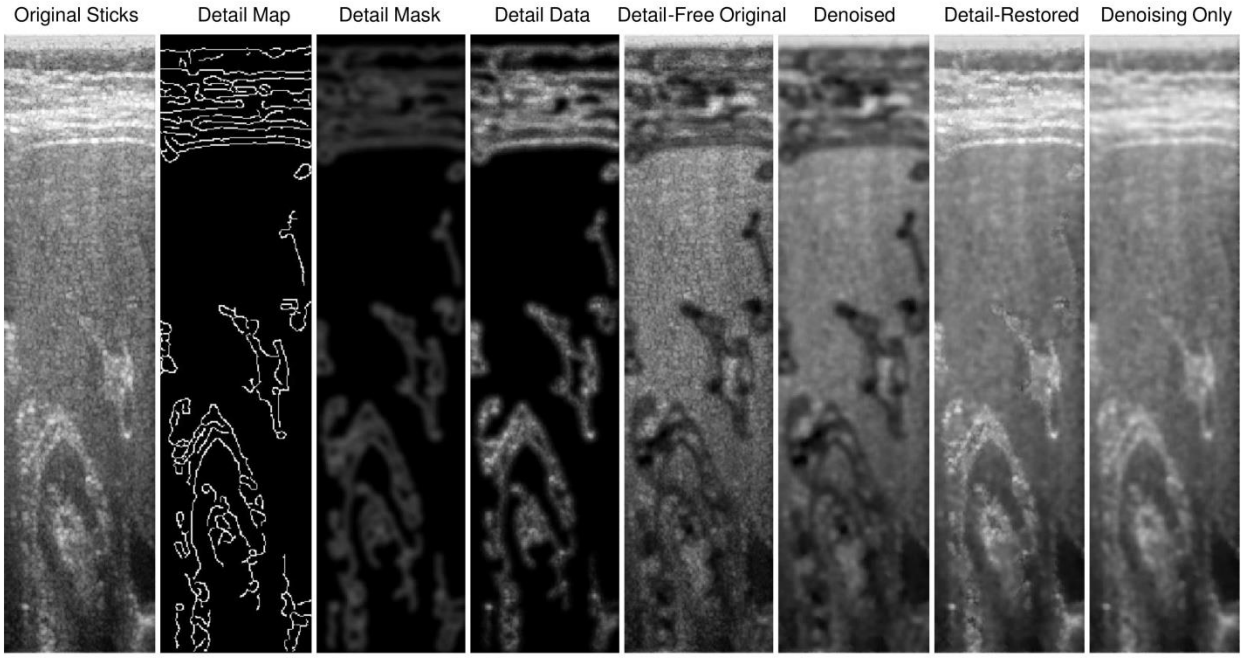

Fig. 1. Illustration of outputs at each block of the proposed edge detail preservation method. The last image to the right illustrates the output of the speckle suppression filter without the new method for comparison.

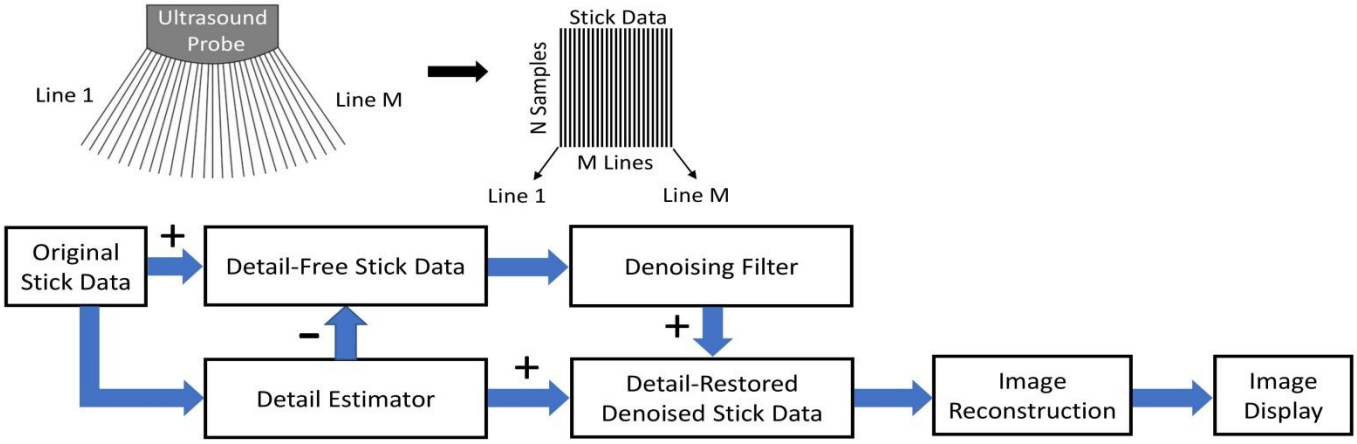

Fig. 2. Block diagram of the proposed edge detail preservation method applied to experimental stick data. The same block diagram applies to images from public databases without need for image reconstruction block.

III. Experimental Verification

The proposed method was verified using collected experimental ultrasound imaging data as well as ultrasound imaging data from publicly available resources. While the latter come in the form of image files encoded using 8-bit image formats such as Joint Photographic Experts Group (JPEG) or Portable Network Graphics (PNG) formats, the collected experimental data come in the form of raw data at a higher quantization rate of 16 bits.

The acquisition of ultrasound imaging data employed the Digison Digital Ultrasound Research system from Mashreq, Egypt. This system, featuring a customized research interface, facilitated image acquisition control with the capability to access and store raw radiofrequency sampled data for each image line. To ensure a representative spectrum of applications, ultrasound array probes, including convex array abdominal probes, small parts linear probes, and tight convex array endo-cavity probes, were utilized. Imaging experiments spanned various clinical applications, conducted on human volunteers and a quality control tissue-mimicking phantom (Multi-Tissue Ultrasound Phantom CIRS Model 040GSE, CIRS Inc., U.S.A.). Each imaging experiment focused on a specific region, employing a designated imaging probe, and entailed collecting 10 images for each application to derive an average, minimizing interference from random noise in speckle reduction filtering. The total number of conducted imaging experiments was 26, yielding a total of 260 images. Fig. 3 illustrates the diversity of images from these 26 experiments. The research interface facilitated raw image data collection at a

sampling rate of 50 M samples/s with 16 bits of quantization. Signal processing involved filter-based Hilbert transformation for peak detection, followed by resampling to yield 512 data samples per line (or stick). The resultant stick data formed a 512×128 array that could subsequently use to reconstruct the final image using scan conversion and interpolation.

The ultrasound imaging data from publicly available resources were obtained from the Breast Ultrasound Imaging (BUSI) database [32] and the B-mode ultrasound imaging cases from Ultrasound Cases training web site [33]. The BUSI database comprises breast sonography images collected from women aged 25 to 75 years in 2018. The dataset encompasses 600 female patients, containing a total of 780 images with an average size of 500 by 500 pixels, provided in PNG format. On the other hand, the data from Ultrasound Cases website are put together through a collaboration between SonoSkills (a provider of ultrasound training in Europe) and FUJIFILM Healthcare Europe. (a manufacturer of medical imaging products, encompassing ultrasound, MRI, and X-ray). The database comprises information gathered from 7678 cases, covering a diverse range of applications, including liver, urinary tract, male reproductive system, gynecology, breast and axilla, as well as musculoskeletal joints and tendons. From this database, a total of 2428 images of size 225 by 300, specifically representing B-mode images, were utilized. Therefore, the total number of images from combining both databases is 3208 images.

The stick data (experimental data) or image (public database data) underwent detection of edge detail mapping using Canny edge detection with thresholds of 0.1 and 0.4 for strong and weak edges, respectively, in both vertical and horizontal directions [27]. Subsequently, a 2D Gaussian spatial filter with a kernel size of three created a mask, which was then multiplied by the original stick data to extract the edge detail content. This content served two purposes: first, subtracted from the original stick data to form detail-free stick data, serving as input for speckle reduction filtering; second, restored to the filtering output to create the final image. The processing steps for experimental stick data are visualized in Fig. 1, with illustrations of the data at each step in Fig. 2. It should be noted that the same diagram applied to public database data with no need for the image reconstruction step. The image quality assessment involved eleven quantitative metrics, comparing output from the speckle suppression filter with and without the edge detail preservation technique. Averaging metrics from the 26 experiments provided reliable comparisons, and standard deviations were computed. Percentage improvement facilitated observation of relative changes across metrics with different numerical ranges. The statistical significance between the two sets of results across experiments was evaluated using the p-value of a two-sample t-test to test the null hypothesis that the observed differences in image quality metrics come from the same distribution where such hypothesis is rejected at a significance level of 0.05.

The final image reconstruction utilized scan conversion and/or interpolation, aligning with array geometry and dimensions to present the image in the correct spatial format. All processing occurred on Matlab 2023a (Mathworks, Inc.) with an educational license from King Abdulaziz University. The computing platform featured an HP Omen 25L personal computer with an 11th generation Intel® Core™ i7-11700F running at 2.50 GHz, using a 64-bit Windows 11 Home Edition, and equipped with 32 GB of RAM.

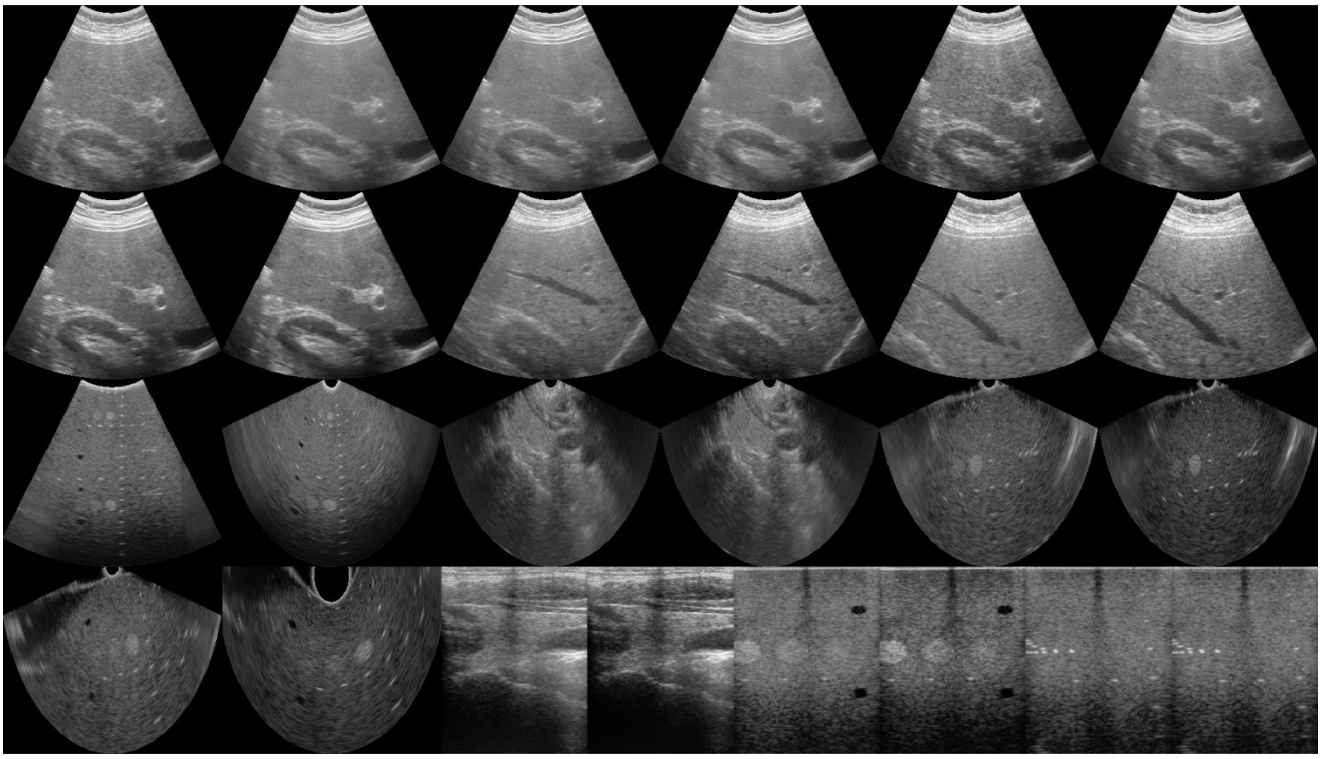

Fig. 3. Visualization of diverse imaging experiments conducted in this investigation.

IV. Results and Discussion

For the experimental data, Fig. 4 presents the output image results stemming from the implementation of the novel edge detail preservation technique, coupled with four illustrative techniques representing the prevailing approaches in speckle reduction for sample applications. Also, Fig. 5 presents magnified versions of parts of the output image results in Fig. 4 to better demonstrate the effect of the new edge preservation method. The considered previous techniques encompass the widely used methods of wavelet denoising [21], [23], relaxed median (RMedian) denoising [14], [15], speckle-reducing anisotropic diffusion (SRAD) [17], [16], [18], and local statistics-based filtering (Lee) [9], [10]. The original images are provided in the left column with the outputs of the four techniques on the first row and their combination with edge detail preservation technique on the second row in each application. As can be observed, the details are sharper with the new method for all techniques and across different applications.

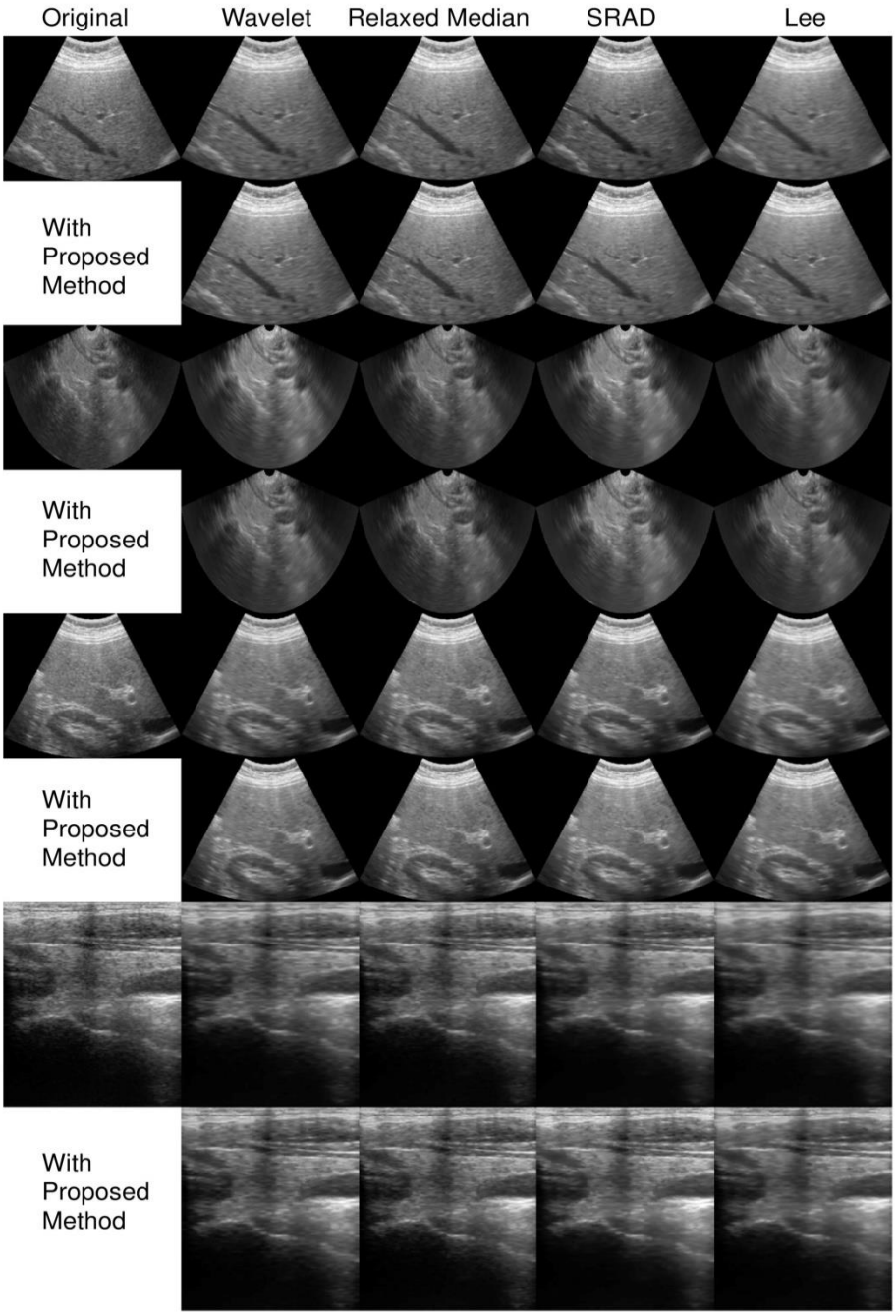

Fig. 4. Diagram showing the output image results from the original speckle suppression techniques (first row of each experiment) and combined with new edge detail preservation method (second row of each experiment) for four example experiments with original image in the left column.

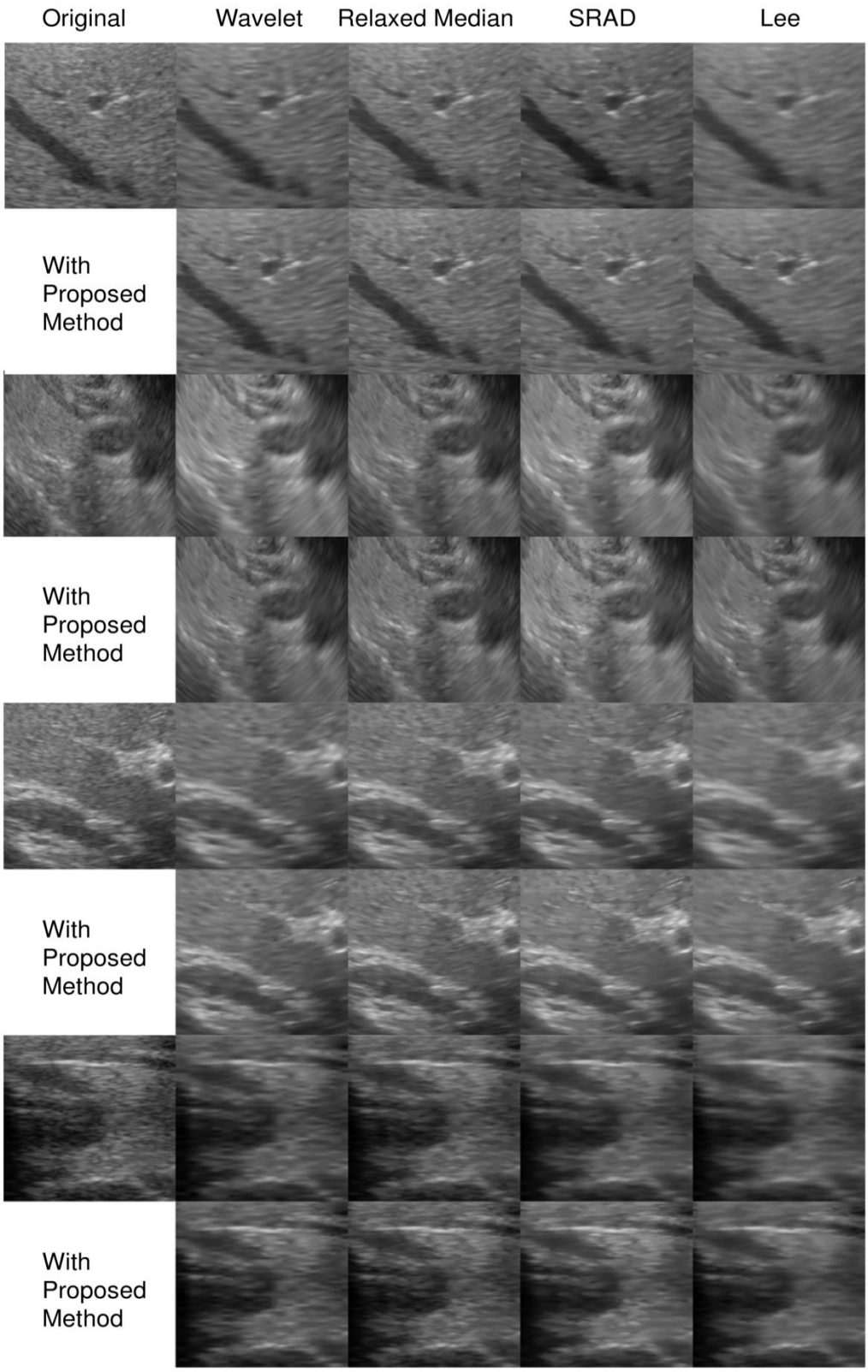

Fig. 5. Magnified parts of the output image of Fig. 4 showing results from the original speckle suppression techniques (first row of each experiment) and combined with new edge detail preservation method (second row of each experiment) for four example experiments with original image in the left column.

TABLE I. IMAGE QUALITY METRICS BEFORE AND AFTER APPLICATION OF PROPOSED EDGE PRESERVATION TO ORIGINAL SPECKLE REDUCTION METHOD, AND ITS STANDARD DEVIATION CALCULATED ACROSS THE SET OF 26 EXPERIMENTS

Quality Metric	Wavelet		Relaxed Median		SRAD		Lee	
	Before	After	Before	After	Before	After	Before	After
Geometric Average Error (GAE)	**3.51** ± 0.61	**2.96** ± 0.49	**2.06** ± 0.35	**1.70** ± 0.29	**4.83** ± 2.28	**3.93** ± 1.56	**3.57** ± 0.57	**2.88** ± 0.47
Mean Squared Error (MSE)	**114.89** ± 31.32	**59.94** ± 19.30	**71.58** ± 16.25	**30.23** ± 9.06	**184.80** ± 156.31	**94.87** ± 63.92	**120.8** ± 30.24	**57.81** ± 18.37
Laplacian Mean Squared Error (LMSE)	**0.99** ± 0.04	**0.67** ± 0.08	**0.94** ± 0.07	**0.66** ± 0.08	**0.62** ± 0.13	**0.41** ± 0.1	**0.95** ± 0.13	**0.61** ± 0.08
Normalized Absolute Error (NAE)	**0.07** ± 0.01	**0.05** ± 0.01	**0.04** ± 0.01	**0.03** ± 0.01	**0.09** ± 0.05	**0.07** ± 0.04	**0.07** ± 0.01	**0.05** ± 0.01
Minkowski Error Metric (β=1)	**7.53** ± 1.22	**5.89** ± 0.97	**4.47** ± 0.67	**3.40** ± 0.57	**10.19** ± 4.82	**7.65** ± 2.93	**7.47** ± 1.14	**5.74** ± 0.94
Minkowski Error Metric (β=3)	**15.82** ± 2.25	**9.24** ± 1.51	**15.08** ± 2.19	**8.55** ± 0.84	**17.00** ± 4.41	**10.71** ± 3.09	**16.11** ± 2.29	**9.15** ± 1.45
Minkowski Error Metric (β=4)	**22.8** ± 4.11	**10.77** ± 1.75	**23.52** ± 3.66	**14.89** ± 1.24	**23.35** ± 4.72	**11.98** ± 3.18	**22.99** ± 4.08	**10.73** ± 1.66
Universal Quality Index (Q)	**0.57** ± 0.04	**0.64** ± 0.04	**0.80** ± 0.04	**0.84** ± 0.04	**0.74** ± 0.08	**0.78** ± 0.08	**0.57** ± 0.05	**0.65** ± 0.05
Structural Similarity Index (SSIN)	**0.66** ± 0.06	**0.72** ± 0.06	**0.84** ± 0.04	**0.87** ± 0.04	**0.81** ± 0.04	**0.85** ± 0.04	**0.66** ± 0.05	**0.74** ± 0.05
Signal-to-Noise Ratio (SNR)	**23.97** ± 1.27	**26.88** ± 1.78	**25.99** ± 1.16	**29.84** ± 2.08	**22.78** ± 3.10	**25.71** ± 3.3	**23.72** ± 1.03	**27.02** ± 1.72
Peak Signal-to-Noise Ratio (PSNR)	**27.65** ± 0.97	**30.41** ± 1.34	**29.27** ± 0.83	**33.25** ± 1.52	**26.40** ± 2.93	**29.39** ± 2.64	**26.83** ± 0.78	**30.48** ± 1.27

TABLE II. AVERAGE PERCENTAGE ALTERATION IN IMAGE QUALITY METRICS FOLLOWING APPLICATION OF PROPOSED EDGE PRESERVATION TO ORIGINAL SPECKLE REDUCTION METHOD AND PERCENTAGE STANDARD DEVIATION ACROSS THE SET OF 26 EXPERIMENTS

Quality Metric	Wavelet	Relaxed Median	SRAD	Lee
Geometric Average Error (GAE)	**-15.65%** ± 5.42	**-17.47%** ± 5.08	**-18.66%** ± 6.49	**-19.31%** ± 4.37
Mean Squared Error (MSE)	**-47.83%** ± 14.48	**-57.77%** ± 18.59	**-48.66%** ± 13.97	**-52.14%** ± 14.63
Laplacian Mean Squared Error (LMSE)	**-32.48%** ± 9.28	**-29.83%** ± 9.61	**-33.08%** ± 9.50	**-36.13%** ± 13.91
Normalized Absolute Error (NAE)	**-19.98%** ± 6.65	**-23.88%** ± 6.94	**-22.52%** ± 9.75	**-23.16%** ± 5.77
Minkowski Error Metric (β=1)	**-19.81%** ± 5.16	**-23.89%** ± 4.81	**-24.94%** ± 7.85	**-23.11%** ± 4.43
Minkowski Error Metric (β=3)	**-41.56%** ± 14.14	**-43.29%** ± 15.34	**-36.98%** ± 18.41	**-43.22%** ± 14.27
Minkowski Error Metric (β=4)	**-52.75%** ± 19.45	**-36.72%** ± 12.99	**-48.7%** ± 24.3	**-53.34%** ± 19.0
Universal Quality Index (Q)	**+11.35%** ± 4.17	**+4.26%** ± 1.62	**+4.88%** ± 2.01	**+14.41%** ± 5.05
Structural Similarity Index (SSIN)	**+9.55%** ± 3.46	**+3.86%** ± 1.45	**+4.26%** ± 2.13	**+11.6%** ± 4.01
Signal-to-Noise Ratio (SNR)	**+12.15%** ± 3.02	**+14.79%** ± 4.54	**+12.86%** ± 4.45	**+13.92%** ± 3.54
Peak Signal-to-Noise Ratio (PSNR)	**+9.97%** ± 2.1	**+13.6%** ± 3.97	**+11.32%** ± 2.16	**+13.59%** ± 3.53

In order to assess the results from the experimental data quantitatively, Table I presents the image quality metrics before and after applying the proposed edge detail preservation method to the original speckle reduction methods and their standard deviations. Table II presents the percentage mean change in image quality metrics after applying the proposed edge detail preservation method to the original speckle reduction methods and their percentage standard deviations. The p-values of statistical significance testing for the two sets of results over the 26 experiments were all significant at the 0.05 level, which supports the hypothesis that the reported changes in image quality metrics are statistically significant. The results indicate that the new edge detail preservation method significantly improves image quality metrics for all speckle reduction methods where error metrics (GAE, MSE, LMSE, NAE, and Minkowski error metrics) become lower and

quality metrics (SNR, PSNR, Q, and SSIN) become higher. To illustrate the actual image quality metric values across different imaging experiments, Fig. 6 shows plots of three example metrics of LMSE, SSIN and Quality, where the metric values from the original speckle suppression alone were plotted as a colored solid line and the combination with the new edge detail preservation method were shown as 'x' marks with the same color. It can be noted that the different applications affect the outcome of speckle suppression techniques in general and that different techniques vary in their performance. The addition of the new edge detail preservation method still resulted in marked improvement across applications and techniques. This suggests its robustness and potential to meet the rigorous demands in real clinical use.

In order to further qualitatively demonstrate the advantage of using the new edge detail preservation method, a zoomed version of the outcomes from using the tissue-mimicking resolution phantom is presented in Fig. 7 where the resolution pins are compared between the outputs from the Lee method with and without the new method. The blurring in the original technique is evident and significant visual improvement is observed after using the new method.

For the ultrasound imaging data from public databases, Table III presents the image quality metrics before and after applying the proposed edge detail preservation method to the original speckle reduction methods and their standard deviations across all 3208 images. Also, Table IV presents the percentage mean change in image quality metrics after applying the proposed edge detail preservation method to the original speckle reduction methods and their percentage standard deviations. The results indicate that the new edge detail preservation method generally improves image quality metrics for all speckle reduction methods where most error metrics (GAE, MSE, LMSE, NAE, and Minkowski error metrics) become lower and quality metrics (SNR, PSNR, Q, and SSIN) become higher. However, the percentage mean change rates of image equality metrics improvement are lower than those in the experimental data particularly for quality metrics (SNR, PSNR, Q, and SSIN). This is most obvious with SRAD technique. This can be explained by the quantization effects on the calculations of the proposed method where edge detection accuracy can be significantly affected, especially for weak edges encountered inside tissues such as edges of blood vessels within the liver. Whereas the experimental data have a quantization level of 16 bits per pixel, the images from public databases come with only 8 bits per pixel, which is substantially lower. This indicates that the proposed method may be better suited to process the raw data rather than the formed, limited quantization ultrasound images.

The advantage of the new edge detail preservation method is that it recognizes the significant body of research already presents in the field of speckle reduction filtering and works to boost the performance of existing methods. This study demonstrated the effectiveness of combing the new method with four existing speckle reduction filters, but its generality and applicability with any other technique are readily evident from its block diagram. The improvement results presented should encourage broader adoption in this area.

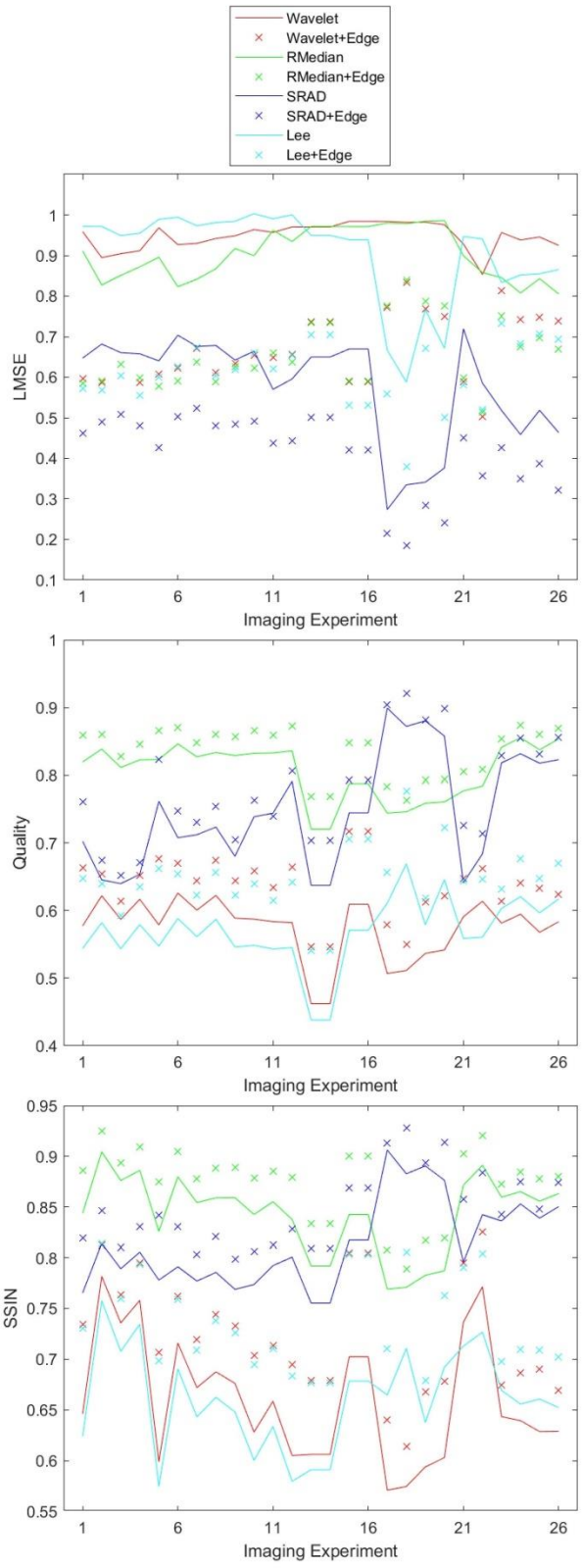

Fig. 6. Performance Comparison of Original Speckle Suppression Techniques with and without New Edge detail Preservation Method as Evaluated by Three Quantitative Image Quality Metrics across 26 Imaging Experiment.

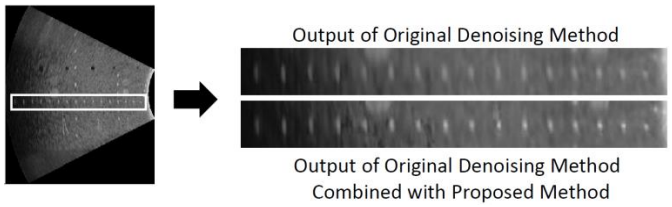

Fig. 7. Qualitative performance comparison of example speckle suppression technique (Lee) with and without new edge detail preservation method where a zoomed part of the output for a tissue mimicking resolution phantom is magnified to demonstrate the improvement.

TABLE III. IMAGE QUALITY METRICS BEFORE AND AFTER APPLICATION OF PROPOSED EDGE PRESERVATION TO ORIGINAL SPECKLE REDUCTION METHOD, AND ITS STANDARD DEVIATION CALCULATED ACROSS ALL IMAGES IN BUSI AND ULTRASOUND CASES DATABASES

Quality Metric	Wavelet		Relaxed Median		SRAD		Lee	
	Before	**After**	**Before**	**After**	**Before**	**After**	**Before**	**After**
Geometric Average Error (GAE)	3.00 ± 0.76	2.77 ± 0.73	1.44 ± 0.33	1.63 ± 0.28	1.97 ± 0.36	1.94 ± 0.32	2.71 ± 0.53	2.49 ± 0.52
Mean Squared Error (MSE)	50.86 ± 26.16	50.09 ± 23.59	901.3 ± 97.52	521.88 ± 205.29	29.02 ± 7.79	27.70 ± 6.80	68.07 ± 19.59	58.38 ± 17.51
Laplacian Mean Squared Error (LMSE)	0.20 ± 0.04	0.15 ± 0.08	0.97 ± 0.07	0.55 ± 0.08	0.14 ± 0.13	0.11 ± 0.1	0.25 ± 0.13	0.17 ± 0.08
Normalized Absolute Error (NAE)	0.1 ± 0.01	0.09 ± 0.01	0.11 ± 0.01	0.08 ± 0.01	0.07 ± 0.05	0.07 ± 0.04	0.10 ± 0.01	0.09 ± 0.01
Minkowski Error Metric (β=1)	5.42 ± 1.44	5.07 ± 1.39	5.87 ± 0.67	4.70 ± 1.03	3.38 ± 0.72	3.76 ± 0.64	5.35 ± 1.07	4.94 ± 1.03
Minkowski Error Metric (β=3)	8.99 ± 2.13	8.41 ± 2.07	59.91 ± 2.78	46.35 ± 8.47	6.54 ± 0.74	6.38 ± 0.68	10.88 ± 1.29	10.00 ± 1.30
Minkowski Error Metric (β=4)	10.5 ± 2.48	9.79 ± 2.41	85.31 ± 3.46	68.26 ± 11.14	7.57 ± 0.75	7.37 ± 0.70	13.71 ± 1.50	12.51 ± 1.53
Universal Quality Index (Q)	0.67 ± 0.09	0.68 ± 0.09	0.86 ± 0.05	0.88 ± 0.06	0.76 ± 0.06	0.75 ± 0.07	0.72 ± 0.06	0.74 ± 0.07
Structural Similarity Index (SSIN)	0.85 ± 0.06	0.87 ± 0.05	0.93 ± 0.04	0.95 ± 0.03	0.88 ± 0.04	0.89 ± 0.03	0.82 ± 0.05	0.84 ± 0.05
Signal-to-Noise Ratio (SNR)	23.30 ± 1.58	23.89 ± 1.71	10.45 ± 1.47	13.2 ± 1.85	25.92 ± 0.89	26.10 ± 0.85	22.17 ± 0.82	22.88 ± 0.96
Peak Signal-to-Noise Ratio (PSNR)	31.21 ± 2.20	31.85 ± 2.29	18.53 ± 0.49	20.48 ± 1.76	33.65 ± 1.20	34.02 ± 1.08	29.67 ± 1.18	30.57 ± 1.33

TABLE IV. AVERAGE PERCENTAGE ALTERATION IN IMAGE QUALITY METRICS FOLLOWING APPLICATION OF PROPOSED EDGE PRESERVATION TO ORIGINAL SPECKLE REDUCTION METHOD AND PERCENTAGE STANDARD DEVIATION ACROSS ALL IMAGES IN BUSI AND ULTRASOUND CASES DATABASES.

Quality Metric	Wavelet	Relaxed Median	SRAD	Lee
Geometric Average Error (GAE)	**-7.78%** ± 2.92	**+12.69%** ± 7.59	**-1.7%** ± 2.32	**-7.93%** ± 3.45
Mean Squared Error (MSE)	**-11.90%** ± 6.42	**-42.10%** ± 16.51	**-4.56%** ± 4.28	**-14.24%** ± 8.68
Laplacian Mean Squared Error (LMSE)	**-24.61%** ± 48.00	**-43.57%** ± 20.61	**-21.78%** ± 56.35	**-30.55%** ± 52.64
Normalized Absolute Error (NAE)	**-6.59%** ± 2.44	**-21.12%** ± 10.59	**-1.43%** ± 2.09	**-7.75%** ± 3.14
Minkowski Error Metric (β=1)	**-6.45%** ± 2.71	**-19.86%** ± 7.19	**-1.71%** ± 2.33	**-7.60%** ± 3.44
Minkowski Error Metric (β=3)	**-6.44%** ± 2.2	**-22.63%** ± 11.51	**-2.44%** ± 1.63	**-8.04%** ± 4.49
Minkowski Error Metric (β=4)	**-6.79%** ± 2.15	**-19.99%** ± 10.77	**-2.64%** ± 1.45	**-8.77%** ± 4.74
Universal Quality Index (Q)	**+2.40%** ± 6.53	**+1.77%** ± 4.77	**-1.09%** ± 5.63	**+2.93%** ± 4.89
Structural Similarity Index (SSIN)	**+2.61%** ± 4.10	**+1.79%** ± 3.97	**+1.04%** ± 4.16	**+11.6%** ± 4.36
Signal-to-Noise Ratio (SNR)	**+2.54%** ± 1.07	**+26.33%** ± 14.43	**+0.68%** ± 0.58	**+3.22%** ± 1.66
Peak Signal-to-Noise Ratio (PSNR)	**+2.05%** ± 0.84	**+10.5%** ± 7.69	**+1.11%** ± 0.50	**+3.04%** ± 1.35

Even though the proposed method is meant to be applied as a tool to complement speckle reduction methods rather than compete with them, it is important to demonstrate that its performance enhancement with classical methods compare well with recent techniques to show its potential. Comparing the presented results to those of [34] using real ultrasound data, the best reported values of PSNR and SSIM are 31.47 and 0.8026 respectively, whereas these same metrics reach 33.25 and 0.87 in the proposed method for experimental data and 34.02 and 0.95 for data from publicly available databases. This particular study shares the utilization of raw ultrasound imaging data as the input to the technique like the proposed method, but the number of images used in that study was reported to be only 20 images out of 366 images that were available in their data source [34], which is much lower than the number of experimental images used in this study of 260 images. Furthermore, simulated speckle noise was added artificially to such real images, which makes such testing data artificial. On the other hand, the study in [37] reported best PSNR and SSIM values of 38.1952 and 0.9770 respectively, which are significantly higher than this work. However, close inspection of the methodology used in that study reveals that such high values were obtained using simulated low variance speckle patterns superimposed on publicly available ultrasound images with very high SNR (small depth of penetration for neural ultrasound images and low attenuation from blood within cardiac images). The reported best results for PSNR and SSIM in that same study from higher speckle variance were 31.3849 and 0.9046 respectively, which are outperformed by the proposed method when applied to publicly available ultrasound images. Furthermore, in [38] the reported best values for PSNR and SSIM were 34.89 and 0.89 respectively, which are again outperformed by the proposed method for publicly available ultrasound images. Hence, the comparison with recent techniques indicates that the proposed method has potential to enhance classical, explainable speckle reduction methods to perform well against more recent deep learning-based methods while maintaining lower complexity.

Given that the new method adds more steps to existing speckle reduction filtering, a concern arises about whether this will affect the real-time performance that is considered very important in ultrasound imaging. In order to estimate the computational complexity of the added blocks in the new method, we need to consider the blocks used to do Canny edge detection (dominated by convolutions), 2D Gaussian filtering (convolution), and final edge detail restoration (addition). For an ultrasound image acquisition M sticks and N samples per line, the combined computational complexity of efficient implementations of these blocks will be $\boldsymbol{O}(MN \log_2(MN))$. This is close to the same order of computations as the image reconstruction process involving scan conversion and interpolation of raw data but with M being the second dimension of the image rather than the smaller number of sticks. Hence, adding the proposed method to the processing chain is not expected to pose any burden for real-time performance especially with current high processing capabilities available in modern digital ultrasound imaging systems. The added complexity of different speckle reduction techniques to be used in combination with the proposed method varies widely across different techniques. To investigate this issue further, we conducted several experiments on Matlab to measure the computation time for the four speckle reduction techniques used in this work along with that of the added processing to implement the proposed method and also the image reconstruction from experimental data for different images sizes. The computational time results are shown in Fig. 8. As can be observed, the computational time of the proposed method scales fairly adheres to the theoretical estimate where it is close to the reconstruction time for smaller image sizes and becomes significantly lower for the commonly used image size of 512. The image reconstruction time increases at a much higher rate at this size because of the much larger number of points in the sector format image that need to be interpolated compared to those at smaller sizes. Furthermore, the proposed method has a significantly lower computational time compared to all speckle reduction methods except the Lee method at this size. Even with the techniques having the largest computation time (Wavelet method), the total computational time needed of 19 ms (Wavelet method) + 11 ms (image reconstruction) + 3 ms (proposed method) = 33 ms at image size of 512×512, offers real-time performance of 30 frames/s on Matlab under Windows operating system without parallel processing or GPU computation. This indicates that real-time performance requirements will be met or exceeded with the dedicated high performance processing platforms used in modern ultrasound imaging systems.

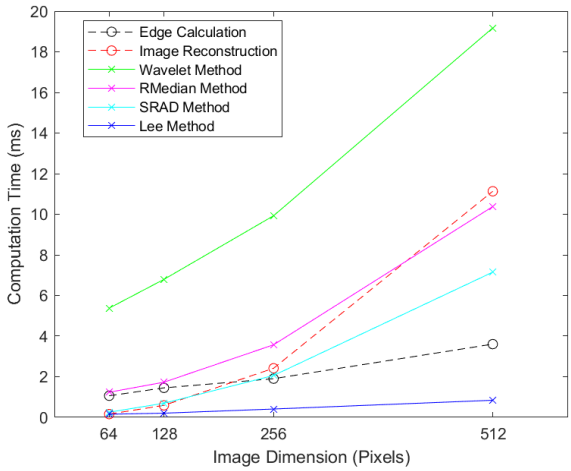

Fig. 8. Computational time for different speckle reduction techniques compared to additional processing for proposed method and image reconstruction for different image sizes.

V. CONCLUSION

This work introduces a novel method designed to augment existing speckle suppression techniques by preserving the edge detail content of images. The process initiates by extracting the edge detail content from the original image. Instead of directly applying the traditional method to the speckle suppression filtering technique, the edge detail content is subtracted from the original image before undergoing the filtering process. Subsequently, this edge detail content is incorporated into the output of the filtering, culminating in the generation of the final image. Experimental validation of this new method was conducted through 26 imaging experiments as well as 3208 ultrasound images from publicly available databases,

employing four representative speckle reduction filters. Real ultrasound imaging data were used to assess the method's performance. Evaluation involved both qualitative comparisons of image appearances and quantitative analyses using eleven image quality metrics. The results affirm the effectiveness of the proposed method and underscore its potential to enhance diagnostic accuracy. Future work includes use for other imaging modalities such as low field MRI or nuclear medicine and combination with other despeckling methods.

ACKNOWLEDGMENT

This project was funded by the Center of Excellence in Intelligent Engineering Systems (CEIES), King Abdulaziz University, Jeddah, under Grant No. (CEIES-16-07-01). The authors, therefore, acknowledge the technical and financial support of King Abdulaziz University.

REFERENCES

[1] P. R. Hoskins, K. Martin, A. Thrush, Diagnostic Ultrasound: Physics and Equipment, 2nd ed., Cambridge University Press, 2010.

[2] C. P. Loizou, C.S. Pattichis, Despeckle Filtering for Ultrasound Imaging and Video, Volume I: Algorithms and Software, 2nd ed., Morgan & Claypool, 2015.

[3] C. B. Burckhardt, "Speckle in ultrasound B-mode scans," IEEE Trans. Sonics Ultrasonics, vol. SU-25, no. 1, pp. 1–6, 1978.

[4] R. F. Wagner, S.W. Smith, J.M. Sandrik, H. Lopez, "Statistics of speckle in ultrasound B-scans," IEEE Trans. Sonics Ultrasonics, vol. 30, pp. 156–163, 1983.

[5] E. Krupinski, H. Kundel, P. Judy, C. Nodine, "The medical image perception society, key issues for image perception research," Radiology, vol. 209, pp. 611–612, 1998.

[6] P. G. Gobbi, Modeling the Optical and Visual Performance of the Human Eye, SPIE Press, 2013.

[7] A. Perperidis, D. Cusack, A. White, N. McDicken, T. MacGillivray, T. Anderson, "Temporal Compounding: A Novel Implementation and Its Impact on Quality and Diagnostic Value in Echocardiography," Ultrasound in Medicine & Biology, vol. 41, no. 6, pp. 1749-1765, 2015.

[8] C. P. Loizou, C. S. Pattichis, Despeckle Filtering for Ultrasound Imaging and Video, Volume II: Selected Applications, 2nd ed., Morgan & Claypool, 2015.

[9] J. S. Lee, "Digital image enhancement and noise filtering by using local statistics," IEEE Trans. Pattern Anal. Mach. Intell., PAMI-2, no. 2, pp. 165–168, 1980.

[10] O. Rubel, V. Lukin, A. Rubel, K. Egiazarian, "Selection of lee filter window size based on despeckling efficiency prediction for sentinel SAR images," Remote Sensing, vol. 13, no. 10, p.1887, 2021.

[11] A. F. de Araujo, C. E. Constantinou, J. Tavares, "Smoothing of ultrasound images using a new selective average filter," Expert Systems with Applications, vol. 60, pp. 96-106, 2016.

[12] J. Saniie, T. Wang, N. Bilgutay, "Analysis of homomorphic processing for ultrasonic grain signal characterization," IEEE Trans. Ultrason. Ferroelectr. Freq. Control, vol. 3, pp. 365–375, 1989.

[13] M. A. Gungor, I. Karagoz, "The homogeneity map method for speckle reduction in diagnostic ultrasound images," Measurement, vol. 68, pp. 100-110, 2015.

[14] A. B. Hamza, P. L. Luque-Escamilla, J. Martínez-Aroza, R. Román-Roldán, "Removing noise and preserving details with relaxed median filters," Journal of mathematical imaging and vision, vol. 11, no. 2, pp.161-177, 1999.

[15] K. Chauhan, R. K. Chauhan, A. Saini, "Enhancement and Despeckling of Echocardiographic Images," In Soft Computing Based Medical Image Analysis, Academic Press, pp. 61-79, 2018.

[16] P. Perona, J. Malik, "Scale-space and edge detection using anisotropic diffusion," IEEE Trans. Pattern Anal. Mach. Intell., vol. 12, no. 7, pp. 629–639, July 1990.

[17] Y. Yongjian, S. T. Acton, "Speckle reducing anisotropic diffusion," IEEE Trans. Image Process., vol. 11, no. 11, pp. 1260–1270, November 2002.

[18] H. Choi, J. Jeong, "Speckle noise reduction for ultrasound images by using speckle reducing anisotropic diffusion and Bayes threshold," Journal of X-ray Science and Technology, vol. 27, no. 5, pp.885-898, 2019.

[19] R. G. Dantas, E. T. Costa, "Ultrasound speckle reduction using modified gabor filters," IEEE Trans Ultrason Ferroelec Freq Cont, vol. 54, no. 3, pp. 530-538, 2007.

[20] K. Z. Abdel-Monem, A. M. Youssef, Y. M. Kadah, "Real-time speckle reduction and coherence enhancement in ultrasound imaging via nonlinear anisotropic diffusion," IEEE Trans. Biomed Eng, vol. 49, no. 9, pp. 997-1014, Sept. 2002.

[21] D. L. Donoho, "Denoising by soft thresholding," IEEE Trans. Inform. Theory, vol. 41, pp. 613–627, 1995.

[22] S. Gupta, R. C. Chauhan, S. C. Sexana, "Wavelet-based statistical approach for speckle reduction in medical ultrasound images," Med Biol Eng Comput, vol. 42, pp. 189–192, 2004.

[23] A. K. Bedi, R. K. Sunkaria, "Ultrasound speckle reduction using adaptive wavelet thresholding," Multidimensional Systems and Signal Processing, vol. 33, no. 2, pp.275-300, 2022.

[24] J. Kang, J. Y. Lee, Y. Yoo, "A new feature-enhanced speckle reduction method based on multiscale analysis for ultrasound B-mode imaging," IEEE Trans Biomed Eng, vol. 63, no. 6, pp. 1178 – 1191, 2016.

[25] J. Zhang, G. Lin, L. Wu, C. Wang, Y. Cheng, "Wavelet and fast bilateral filter based de-speckling method for medical ultrasound images," Biomed Sig Proc Cont, vol. 18, pp. 1-10, 2015.

[26] B. A. Abrahim, Z. A. Mustafa, I. A. Yassine, N. Zayed, Y. M. Kadah, "Hybrid Total Variation and Wavelet Thresholding Speckle Reduction for Medical Ultrasound Imaging," J Med Imag Health Inform, vol. 2, pp. 114-124, 2012.

[27] J. Canny, "A Computational Approach to Edge Detection," IEEE Transactions on Pattern Analysis and Machine Intelligence, vol. PAMI-8, no. 6, pp. 679-698, 1986.

[28] A. M. Eskicioglu, P.S. Fisher, "Image quality measures and their performance," IEEE Trans. On Communications, vol. 43, no. 12, pp. 2959-2965, 1995.

[29] Z. Wang, A. Bovik, H. Sheikh, E. Simoncelli, "Image quality assessment: From error measurement to structural similarity," IEEE Trans. Image Process., vol. 13, no. 4, pp. 600–612, April 2004.

[30] Z. Wang and A. Bovik, "A universal quality index," IEEE Signal Process. Lett., vol. 9, no. 3, pp. 81–84, March 2002.

[31] D. Sakrison, "On the role of observer and a distortion measure in image transmission," IEEE Trans. On Communications, vol. 25, pp. 1251–1267, November 1977.

[32] W. Al-Dhabyani, M. Gomaa, H. Khaled, and A. Fahmy. "Dataset of breast ultrasound images," Data in Brief, vol. 28, p.104863, 2020.

[33] https://www.ultrasoundcases.info [Accessed: December 13, 2023].

[34] R. Reyes-Reyes, G. H. Aranda-Bojorges, B. P. Garcia-Salgado, V. Ponomaryov, C. Cruz-Ramos, and S. Sadovnychiym, "Despeckling of Ultrasound Images Using Block Matching and SVD in Sparse Representation," Sensors, vol. 22, no. 14, p. 5113, 2022.

[35] Y. M. Kadah, A. F. Elnokrashy, U. M. Alsaggaf, and A. M. Youssef. "Principal Component Analysis Based Hybrid Speckle Noise Reduction Technique for Medical Ultrasound Imaging," International Journal of Advanced Computer Science and Applications, vol. 13, no. 12, pp. pp. 459-468, 2022.

[36] Y. M. Kadah, A. F. Elnokrashy, U. M. Alsaggaf, and A. M. Youssef. "Speckle Reduction in Medical Ultrasound Imaging based on Visual Perception Model." International Journal of Advanced Computer Science and Applications, vol. 13, no. 11, pp. 575-581, 2022.

[37] Y. Chen, and Z. Guo. "TranSpeckle: An edge-protected transformer for medical ultrasound image despeckling," IET Image Processing, vol. 17, pp. 4014–4027, 2023.

[38] G. Karthiha, and S. Allwin, "Speckle Noise Suppression in Ultrasound Images Using Modular Neural Networks." Intelligent Automation & Soft Computing, vol. 35, no. 2, pp. 1753-1765, 2023.